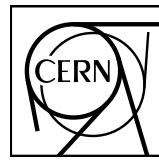


EUROPEAN ORGANIZATION FOR NUCLEAR RESEARCH



CERN-EP-2015-XXX
Day Month 2015

ΛK femtoscopy in Pb-Pb collisions at $\sqrt{s_{NN}} = 2.76 \text{ TeV}$

ALICE Collaboration*

Abstract

We present our femtoscopy analysis of ΛK correlations in Pb-Pb collisions at $\sqrt{s_{NN}} = 2.76 \text{ TeV}$ from ALICE. The femtoscopic correlations result from strong final-state interactions, and are fit with a parametrization based on a model by Lednicky and Lyuboshitz. This allows us to both characterize the emission source and measure the scattering parameters for the particle pairs. We observe a large difference in the ΛK^+ and ΛK^- correlations in pairs with low relative momenta. This might suggest an effect arising from different quark-antiquark interactions between the pairs ($s\bar{s}$ in ΛK^+ and $u\bar{u}$ in ΛK^-), or from different net strangeness for each system.

© 2015 CERN for the benefit of the ALICE Collaboration.

Reproduction of this article or parts of it is allowed as specified in the CC-BY-4.0 license.

*See Appendix C for the list of collaboration members

1 Introduction

Femtoscopy is an experimental method used to study the space-time characteristic of the particle emitting sources in relativistic particle collisions [1]. With this method, two(or many)-particle relative-momentum correlation functions are used to connect the final-state momentum distributions to the space-time distributions of particle emission at freeze-out. The correlation functions are sensitive to quantum statistics, as well as strong and Coulomb final-state interactions (FSI). In addition to characterizing the source region, femtoscopy offers a unique opportunity to measure nuclear scattering parameters, many of which are difficult, if not impossible, to measure otherwise. In many pair systems, the contributions to the correlation function from quantum statistics and/or the Coulomb interaction overwhelm that of the strong interaction, making it difficult to extract scattering information. In this article, we study npn-identical particle pairs, with at least one electrically neutral particle in the pair. Therefore, quantum statistics and the Coulomb interaction do not contribute, giving us a clear signal from the strong interaction.

Femtoscopy analyses of pion, kaons, and protons have revealed a trend of decreasing source radii with increasing transverse mass, $m_T^2 = (\frac{m_{\text{inv}}}{2})^2 + k_T^2$, where $k_T = \frac{1}{2}|\mathbf{p}_{T,1} + \mathbf{p}_{T,2}|$. This is interpreted as a signature of hydrodynamic flow, and therefore deconfined quark matter, in the heavy-ion collisions.

We observe mT-scaling. However, remember plot is for identical particle femtoscopy. When dealing with ΛK, don't necessarily expect exact same trend. mT-scaling has to do with hydro, and single particle distributions. With femtoscopy, we are dealing with pairs of particles. If we look at ΛK as a function of mT, we certainly would expect a decreasing behavior with increasing mT, but the exact shape may not be same of pipi, kk, pp, etc.

Motivation for comparing studies with different particle species, and for ΛK in particular.

This paper presents results from a femtoscopic analysis of ΛK correlations in Pb-Pb collisions at $\sqrt{s_{\text{NN}}} = 2.76$ TeV by the ALICE experiment at the LHC. All pair combinations of Λ and $\bar{\Lambda}$ with K^+ , K^- and K_S^0 are analyzed. The femtoscopic correlations are the result of strong final-state interactions, and are fit with a parametrization based on a model by R. Lednický and V. L. Lyuboshitz [2]. This allows us to both characterize the emission source and measure the scattering parameters for the particle pairs. We observe a large difference in the $\Lambda K^+ (\bar{\Lambda} K^-)$ and $\Lambda K^- (\bar{\Lambda} K^+)$ correlations in pairs with low relative momenta ($k^* \lesssim 100$ MeV). The results suggest an effect arising from different quark-antiquark interactions in the pairs, i.e. $s\bar{s}$ in $\Lambda K^+ (\bar{\Lambda} K^-)$ and $u\bar{u}$ in $\Lambda K^- (\bar{\Lambda} K^+)$. The femtoscopic radii, λ parameters, and scattering parameters are extracted from...

The organization of this paper is as follows. Sec. 2, Sec. 3, Sec. 4, Sec. 5.

2 Data Analysis

The dataset analyzed is from Pb-Pb collisions at $\sqrt{s_{\text{NN}}} = 2.76$ TeV at the LHC measured by the ALICE detector [3]. Approximately 40 million combined central, semi-central, and minimum bias events were analyzed. The events were classified according to their centrality determined using the measured amplitudes in the V0 detectors [4]. In order for an event to be included in the analysis, the z-position of the reconstructed event vertex must be within 10 cm of the center of the ALICE detector, and the event must contain at least one particle of each type from the pair of interest (ex. for ΛK^+ analysis, an accepted event must contain at least one Λ and at least one K_S^0). Charged particle tracking was performed using the Time Projection Chamber (TPC) [5] (Tom) or [6] (1dPionKaonProton) and the Inner Tracking System [3]. The ITS allows for high spatial resolution in determining the primary (collision) vertex. The determination of the momenta of the tracks was performed using tracks reconstructed with the TPC only and constrained to the primary vertex.

Particle identification (PID) for reconstructed tracks was carried out using both the TPC and Time-of-

Flight (TOF) detector [7, 8] (Tom) or [9] (1dPionKaonProton) in the pseudorapidity range $|\eta| < 0.8$. For TPC PID, a parametrized Bethe-Bloch formula was used to calculate the specific energy loss $\langle dE/dx \rangle$ in the detector expected for a particle with a given mass and momentum. For TOF PID, the particle mass was used to calculate the expected time-of-flight as a function of track length and momentum. For each PID method, a value ($N\sigma$) was assigned to each track denoting the number of standard deviations between the measured track information and calculated values. This procedure was repeated for four "particle species hypotheses" - electron, pion, kaon, and proton-, and, for each hypothesis, a different $N\sigma$ value was obtained per detector.

2.1 V0 selection

$\Lambda(\bar{\Lambda})$ and K_S^0 particles are electrically neutral, and cannot be directly detected, but must instead be reconstructed through detection of their decay products, or daughters. This process is illustrated in Figure 1. In general, particles which are topologically reconstructed in this fashion are called V0 particles.

Daughter tracks selected by requiring a minimum impact parameter with respect to primary vertex. Positive and negative tracks combined to form a pair. V0 vertex is then point of closest approach of tracks. This distance is used for additional quality criterion.

V0 momentum calculated as sum of daughters momenta. Minimum transverse momentum to reduce contribution from fakes. Selection on opening angle between V0 momentum and vector pointing from primary vertex to secondary V0 decay vertex. Finally, invariant mass cut.

To avoid auto-correlation, all candidates checked for shared daughters. If shared daughters, how do I decide which V0 to keep? (Cosine of pointing angle?)

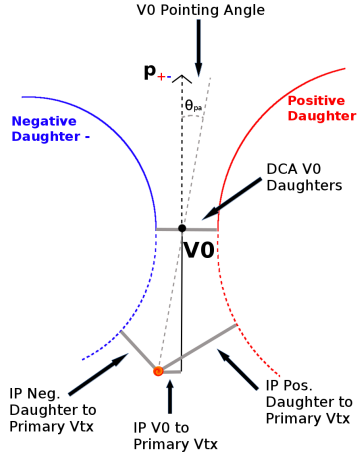


Fig. 1: V0 Reconstruction

The decay channel $\Lambda \rightarrow p\pi^-$ ($\bar{\Lambda} \rightarrow \bar{p}\pi^+$) was used for the identification of $\Lambda(\bar{\Lambda})$ hyperons, and $K_S^0 \rightarrow \pi^+\pi^-$ for the identification of K_S^0 mesons. Main cuts shown in Tables 1 and 2. PID for pion daughters using both TPC (what momenta?) and TOF (what momenta?). Figure 2(b) shows $\pi^+\pi^-$ invariant mass distribution showing K_S^0 peak.

Figure 2 shows the invariant mass (m_{inv}) distribution of all Λ and K_S^0 candidates (in the 0-10% centrality bin) immediately before the final invariant mass cut. These distributions (and similar for $\bar{\Lambda}$) are used to calculate the collections' purities (defined in Eq. 1). The Λ and $\bar{\Lambda}$ purities were found to be $\approx 95\%$. The neutral kaon purity was found to be $\approx 98\%$.

Shared daughter cut iterates through V0 collection to ensure that no daughter is used in more than one V0 candidate.

On occasion, $\Lambda(\bar{\Lambda})$ particles are misidentified as K_S^0 , and vice versa. To attempt to remove these contaminations without throwing away good candidates, we impose a set of misidentification cuts. The intent of these cuts is to judge whether a candidate is more likely a $\Lambda(\bar{\Lambda})$ or a K_S^0 .

For a given V0, we calculate the mass assuming different identities (Λ , $\bar{\Lambda}$, K_S^0); the mass assuming K_S^0 hypothesis ($m_{\text{inv}, K_S^0 \text{ Hypothesis}}$) is calculated assuming both of the daughters are pions, the mass assuming Λ hypothesis ($m_{\text{inv}, \Lambda \text{ Hypothesis}}$) is calculated assuming the positive daughter is a proton and the negative daughter a pion, and the mass assuming $\bar{\Lambda}$ hypothesis ($m_{\text{inv}, \bar{\Lambda} \text{ Hypothesis}}$) is calculated assuming the positive daughter is a pion and the negative an anti-proton. In addition to the notation just introduced, in the following, m_{PDG, K_S^0} and $m_{\text{PDG}, \Lambda(\bar{\Lambda})}$ denote the particle masses of the K_S^0 and $\Lambda(\bar{\Lambda})$, respectively, as recorded by the Particle Data Group [10].

For $\Lambda(\bar{\Lambda})$ selection, a candidate is rejected if all of the following criteria are satisfied:

1. $|m_{\text{inv}, K_S^0 \text{ Hypothesis}} - m_{\text{PDG}, K_S^0}| < 9.0 \text{ MeV}/c^2$
2. Daughter particles pass daughter cuts intended for K_S^0 reconstruction
 - (a) Λ selection
 - i. p daughter passes π^+ cuts intended for K_S^0 reconstruction
 - ii. π^- daughter passes π^- cuts intended for K_S^0 reconstruction.
 - (b) $\bar{\Lambda}$ selection
 - i. π^+ daughter passes π^+ cuts intended for K_S^0 reconstruction
 - ii. \bar{p} daughter passes π^- cuts intended for K_S^0 reconstruction.
3. $|m_{\text{inv}, K_S^0 \text{ Hypothesis}} - m_{\text{PDG}, K_S^0}| < |m_{\text{inv}, \Lambda(\bar{\Lambda}) \text{ Hypothesis}} - m_{\text{PDG}, \Lambda(\bar{\Lambda})}|$

Similarly, for K_S^0 selection, a candidate is rejected if all of the following criteria are satisfied for the Λ case, or for the $\bar{\Lambda}$ case:

1. $|m_{\text{inv}, \Lambda(\bar{\Lambda}) \text{ Hypothesis}} - m_{\text{PDG}, \Lambda(\bar{\Lambda})}| < 9.0 \text{ MeV}/c^2$
2. Daughter particles pass daughter cuts intended for $\Lambda(\bar{\Lambda})$ reconstruction
 - (a) π^+ daughter passes p(π^+) daughter cut intended for $\Lambda(\bar{\Lambda})$ reconstruction
 - (b) π^- daughter passes π^- (\bar{p})
3. $|m_{\text{inv}, \Lambda(\bar{\Lambda}) \text{ Hypothesis}} - m_{\text{PDG}, \Lambda(\bar{\Lambda})}| < |m_{\text{inv}, K_S^0 \text{ Hypothesis}} - m_{\text{PDG}, K_S^0}|$

In order to obtain a true and reliable signal, one must ensure good purity of the V0 collection. The purity of the collection is calculated as:

$$\text{Purity} = \frac{\text{Signal}}{\text{Signal} + \text{Background}} \quad (1)$$

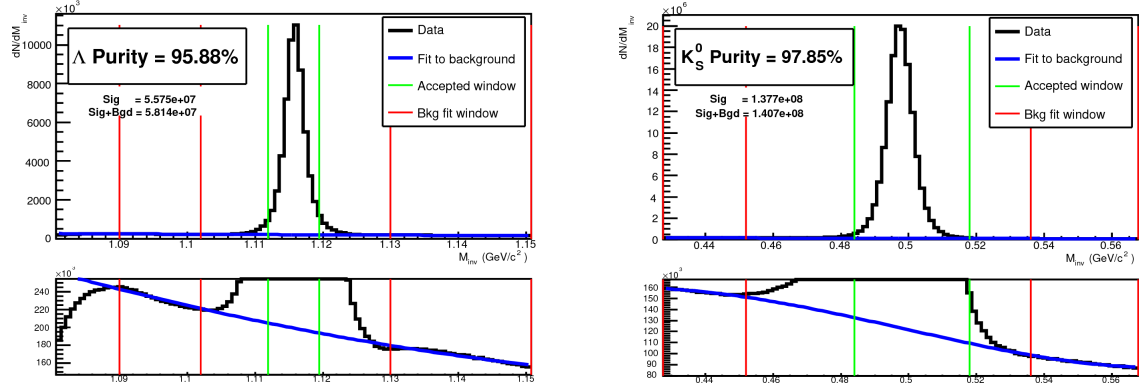
To obtain both the signal and background, the invariant mass distribution (m_{inv}) of all V0 candidates must be constructed immediately before the final invariant mass cut. Examples of such distributions can be found in Figure 2]. It is vital that this distribution be constructed immediately before the final m_{inv} cut, otherwise it would be impossible to estimate the background. As shown in Figure 2, the background is fit (with a polynomial) outside of the peak region of interest to obtain an estimate for the background within the region. Within the m_{inv} cut limits, the background is the region below the fit while the signal is the region above the fit.

Λ selection	
Transverse momentum p_T	$> 0.4 \text{ GeV}/c$
$ \eta $	< 0.8
$ m_{\text{inv}} - m_{\text{PDG}} $	$< 3.8 \text{ MeV}$
DCA to primary vertex	$< 0.5 \text{ cm}$
Cosine of pointing angle	> 0.9993
Decay Length	$< 60 \text{ cm}$
Daughter Cuts (π and p)	
$ \eta $	< 0.8
DCA πp Daughters	$< 0.4 \text{ cm}$
π-specific cuts	
p_T	$> 0.16 \text{ GeV}/c$
DCA to primary vertex	$> 0.3 \text{ cm}$
TPC and TOF $N\sigma$ Cuts	
$p < 0.5 \text{ GeV}/c$	$N\sigma_{\text{TPC}} < 3$
$p > 0.5 \text{ GeV}/c$ if TOF & TPC available	$N\sigma_{\text{TPC}} < 3$
	$N\sigma_{\text{TOF}} < 3$
else	$N\sigma_{\text{TOF}} < 3$
p-specific cuts	
p_T	$> 0.5(p) [0.3(\bar{p})] \text{ GeV}/c$
DCA to primary vertex	$> 0.1 \text{ cm}$
TPC and TOF $N\sigma$ Cuts	
$p < 0.8 \text{ GeV}/c$	$N\sigma_{\text{TPC}} < 3$
$p > 0.8 \text{ GeV}/c$ if TOF & TPC available	$N\sigma_{\text{TPC}} < 3$
	$N\sigma_{\text{TOF}} < 3$
else	$N\sigma_{\text{TOF}} < 3$

Table 1: Λ selection

K_S^0 selection	
Transverse momentum p_T	$> 0.2 \text{ GeV}/c$
$ \eta $	< 0.8
$m_{\text{PDG}} - 13.677 \text{ MeV} < m_{\text{inv}} < m_{\text{PDG}} + 2.0323 \text{ MeV}$	
DCA to primary vertex	$< 0.3 \text{ cm}$
Cosine of pointing angle	> 0.9993
Decay Length	$< 30 \text{ cm}$
π^\pm Daughter Cuts	
p_T	$> 0.15 \text{ GeV}/c$
$ \eta $	< 0.8
DCA $\pi^+ \pi^-$ Daughters	$< 0.3 \text{ cm}$
DCA to primary vertex	$> 0.3 \text{ cm}$
TPC and TOF $N\sigma$ Cuts	
$p < 0.5 \text{ GeV}/c$	$N\sigma_{\text{TPC}} < 3$
$p > 0.5 \text{ GeV}/c$ if TOF & TPC available	$N\sigma_{\text{TPC}} < 3$
	$N\sigma_{\text{TOF}} < 3$
else	$N\sigma_{\text{TOF}} < 3$

Table 2: K_S^0 selection



(a) $p\pi^-$ invariant mass distribution where the Λ peak is seen. (b) $\pi^+\pi^-$ invariant mass distribution where the K_S^0 peak is seen.

Fig. 2: Invariant mass (m_{inv}) distribution of all Λ 2(a) and K_S^0 2(b) candidates immediately before the final invariant mass cut. The bottom figures are zoomed to show the background with fit. The vertical green lines represent the m_{inv} cuts used in the analyses, the red vertical lines delineate the region over which the background was fit, and the blue line shows the background fit. These distributions (or similar, for $\bar{\Lambda}$) are used to calculate the collection purities, $\text{Purity}(\Lambda) \approx \text{Purity}(\bar{\Lambda}) \approx 95\%$, and $\text{Purity}(K_S^0) \approx 98\%$.

2.2 K^\pm selection

The single-particle selection criteria used to select charged kaon candidates are summarized in Table 3. K^\pm identification utilized both TPC (what momenta?) and TOF (what momenta?). Figure 3 shows dE/dx .

Selection on number of reconstructed TPC clusters ensure quality of track, ensure good pT resolution at large momenta and to remove fake tracks. DCA in transverse and longitudinal to enhance number produced at primary vertex. Low pT (for protons!! True for others too?) to minimize the fraction originating from interaction of primary particles with detector material. High pT to ensure purity, due to decreasing separation power of combined TPC and TOF.

The purity of the K^\pm collections was estimated from a Monte-Carlo (MC) study based on HIJING [11] simulations using GEANT3 [12] to model particle transport through the ALICE detectors. In these simulations, the true identity of each reconstructed K^\pm particle is known; therefore, the purity may be estimated as:

$$\text{Purity}(K^\pm) = \frac{N_{\text{true}}}{N_{\text{reconstructed}}} \quad (2)$$

$$\text{Purity}(K^+) \approx \text{Purity}(K^-) \approx 97\%$$

2.3 Pair Selection

I suppose I should probably briefly explain how pairs are formed?

It is important to obtain true particle pairs in the analysis. In particular, contamination from pairs constructed with split or merged tracks, and pairs sharing daughters, can introduce an artificial signal into the correlation function, obscuring the actual physics. In an effort to remove contamination, we impose two main two-particle cuts: a shared daughter cut, and an average separation cut.

The purpose of the shared daughter cut is to ensure the first particle in the pair is unique from the second. For pairs formed of two V0s (i.e. ΛK_S^0), this cut is implemented by removing all pairs which share a

K[±] selection		
Transverse momentum p_T		$0.14 < p_T < 1.5 \text{ GeV}/c$
$ \eta $		< 0.8
Transverse DCA to primary vertex		$< 2.4 \text{ cm}$
Longitudinal DCA to primary vertex		$< 3.0 \text{ cm}$
TPC and TOF N σ Cuts		
$p < 0.4 \text{ GeV}/c$		$N_{\sigma K, \text{TPC}} < 2$
$0.4 < p < 0.45 \text{ GeV}/c$		$N_{\sigma K, \text{TPC}} < 1$
$0.45 < p < 0.80 \text{ GeV}/c$		$N_{\sigma K, \text{TPC}} < 3$ $N_{\sigma K, \text{TOF}} < 2$
$0.80 < p < 1.0 \text{ GeV}/c$		$N_{\sigma K, \text{TPC}} < 3$ $N_{\sigma K, \text{TOF}} < 1.5$
$p > 1.0 \text{ GeV}/c$		$N_{\sigma K, \text{TPC}} < 3$ $N_{\sigma K, \text{TOF}} < 1$
Electron Rejection		Reject if $N_{\sigma e^-, \text{TPC}} < 3$
Pion Rejection: Reject if:		
$p < 0.65 \text{ GeV}/c$	if TOF and TPC available	$N_{\sigma \pi, \text{TPC}} < 3$ $N_{\sigma \pi, \text{TOF}} < 3$
	else	$p < 0.5 \text{ GeV}/c$ $0.5 < p < 0.65 \text{ GeV}/c$
$0.65 < p < 1.5 \text{ GeV}/c$		$N_{\sigma \pi, \text{TPC}} < 5$ $N_{\sigma \pi, \text{TOF}} < 3$
$p > 1.5 \text{ GeV}/c$		$N_{\sigma \pi, \text{TPC}} < 5$ $N_{\sigma \pi, \text{TOF}} < 2$

Table 3: K[±] selection

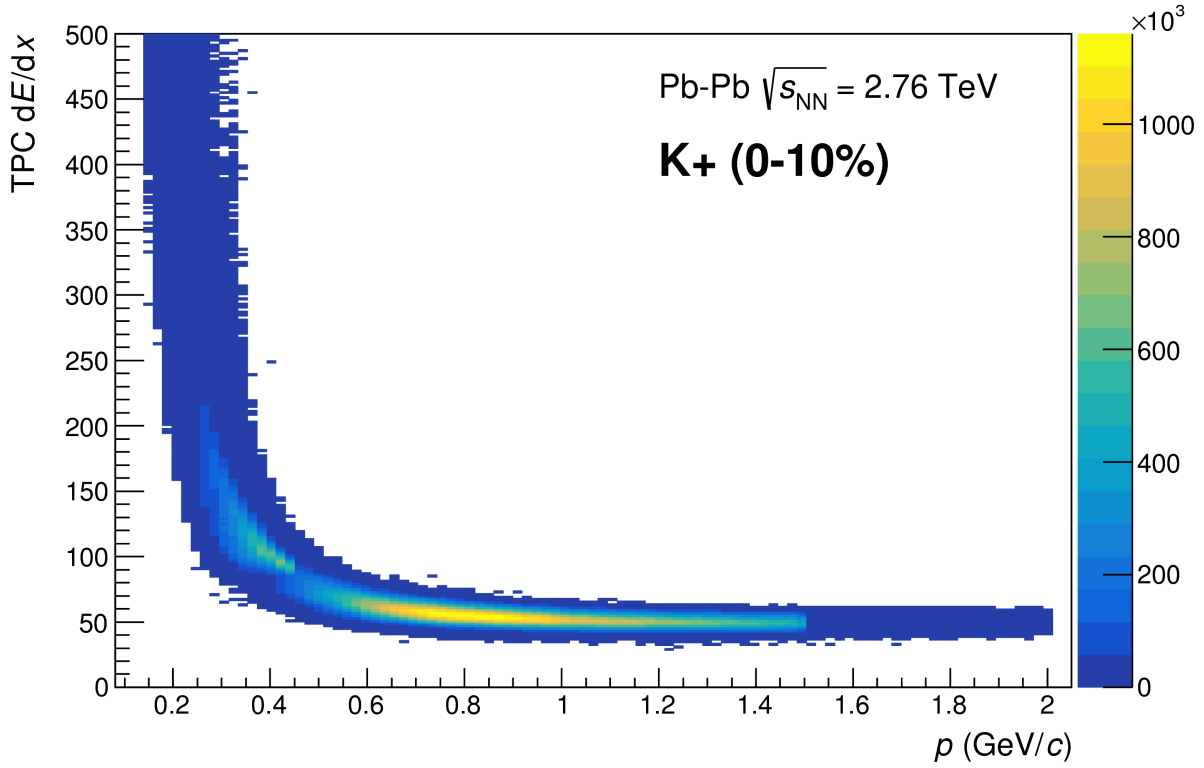


Fig. 3: A figure caption. The figure captions are automatically numbered.

daughter (ex. in ΛK_S^0 analysis, if the Λ and K_S^0 in a potential pair claim the same π^- daughter, the pair is excluded from the analysis). For a pair formed of a single V0 and a charged track (i.e. ΛK^\pm), the cut removes all pairs in which the charged track is also claimed as a daughter of the V0. This mistake could only occur if, for instance, a K^\pm is misidentified as a π or p either in the V0 reconstruction or in the K^\pm selection.

The purpose of the average separation cut is to remove splitting and merging effects. How do we estimate the cut values? How do we implement the cut?

For the $\Lambda(\bar{\Lambda})K_S^0$ analysis, the average separation for like-charge daughters must be greater than 6.0 cm. We enforce no cut for unlike-charge daughters. For example, we impose this cut in a ΛK_S^0 analysis on the p daughter of the Λ and the π^+ daughter of the K_S^0 . For the ΛK^\pm analyses, the average separation between the $\Lambda(\bar{\Lambda})$ daughter (sharing the same charge as the K^\pm) and the K^\pm is 8.0 cm. We enforce no cut for unlike signs. For a ΛK^+ analysis, we impose this cut between the p daughter of the Λ and the K^+ in the pair.

3 Construction of correlation functions and fitting

The event mixing was handled by the AliFemtoVertexMultAnalysis class, which only mixes events with like vertex position and centrality. The following criteria were used for event mixing:

- Number of events to mix = 5
- Vertex position bin width = 2 cm
- Centrality bin width = 5

General remarks about formaton of correlation functions and what information they provide.

This analysis studies the momentum correlations of both ΛK and ΞK pairs using the two-particle correlation function, defined as $C(k^*) = A(k^*)/B(k^*)$, where $A(k^*)$ is the signal distribution, $B(k^*)$ is the reference (or background) distribution, and k^* is the momentum of one of the particles in the pair rest frame. In practice, $A(k^*)$ is constructed by binning in k^* pairs from the same event. Ideally, $B(k^*)$ is similar to $A(k^*)$ in all respects excluding the presence of femtoscopic correlations [1]; as such, $B(k^*)$ is used to divide out the phase-space effects, leaving only the femtoscopic effects in the correlation function.

In practice, $B(k^*)$ is obtained by forming mixed-event pairs, i.e. particles from a given event are paired with particles from $N_{mix}(= 5)$ other events, and these pairs are then binned in k^* . In forming the background distribution, it is important to mix only similar events; mixing events with different phase-spaces can lead to artificial signals in the correlaton function. Therefore, in this analysis, we mix events with primary vertices within 2 cm and centralities within 5% of each other. Also note, a vertex correction is also applied to each event, which essentially recenters the the primary vertices to $z = 0$.

This analysis presents correlation functions for three centrality bins (0-10%, 10-30%, and 30-50%), and is currently pair transverse momentum ($k_T = 0.5|\mathbf{p}_{T,1} + \mathbf{p}_{T,2}|$) integrated (i.e. not binned in k_T). The correlation functions are constructed separately for the two magnetic field configurations, and are combined using a weighted average:

$$C_{combined}(k^*) = \frac{\sum_i w_i C_i(k^*)}{\sum_i w_i} \quad (3)$$

where the sum runs over the correlation functions to be combined, and the weight, w_i , is the number of numerator pairs in $C_i(k^*)$. Here, the sum is over the two field configurations.

Figures 4(a), 4(b), and 4(c) show the correlation functions for all centalities studied for $\Lambda K^+(\bar{\Lambda} K^-)$, $\Lambda K^-(\bar{\Lambda} K^+)$, and $\Lambda K_S^0(\bar{\Lambda} K_S^0)$, respectively. All were normalized in the range $0.32 < k^* < 0.4$ GeV/c.

3.1 Fit Function

Ya boys Lednicky and Lyuboshitz!

The two-particle relative momentum correlation function may be written theoretically by the Koonin-Pratt equation [13, 14]:

$$C(\mathbf{k}^*) = \int S(\mathbf{r}^*) |\Psi_{\mathbf{k}^*}(\mathbf{r}^*)|^2 d^3 \mathbf{r}^* \quad (4)$$

where $S(\mathbf{r}^*)$ is the pair source distribution, $\Psi_{\mathbf{k}^*}(\mathbf{r}^*)$ is the two-particle wave-function, and k^* is the momentum of one particle in the pair rest frame. In the absence of Coulomb effects, and assuming a spherically Gaussian source of width R , and s-wave scattering, the 1D femtoscopic correlation function can be calculated analytically using:

$$C(k^*) = 1 + C_{QI}(k^*) + C_{FSI}(k^*) \quad (5)$$

C_{QI} describes plane-wave quantum interference:

$$C_{QI}(k^*) = \alpha \exp(-4k^{*2}R^2) \quad (6)$$

where $\alpha = (-1)^{2j}/(2j+1)$ for identical particles with spin j , and $\alpha = 0$ for non-identical particles. Obviously, $\alpha = 0$ for all analyses presented in this note. C_{FSI} describes the s-wave strong final state interaction between the particles:

$$\begin{aligned} C_{FSI}(k^*) &= (1 + \alpha) \left[\frac{1}{2} \left| \frac{f(k^*)}{R} \right|^2 \left(1 - \frac{d_0}{2\sqrt{\pi}R} \right) + \frac{2\mathbb{R}f(k^*)}{\sqrt{\pi}R} F_1(2k^*R) - \frac{\mathbb{I}f(k^*)}{R} F_2(2k^*R) \right] \\ f(k^*) &= \left(\frac{1}{f_0} + \frac{1}{2} d_0 k^{*2} - ik^* \right)^{-1}; \quad F_1(z) = \int_0^z \frac{e^{x^2-z^2}}{z} dx; \quad F_2(z) = \frac{1-e^{-z^2}}{z} \end{aligned} \quad (7)$$

where R is the source size, $f(k^*)$ is the s-wave scattering amplitude, f_0 is the complex scattering length, and d_0 is the effective range of the interaction.

An additional parameter λ is typically included in the femtoscopic fit function to account for the purity of the pair sample. In the case of no residual correlations (to be discussed in Section 3.3, the fit function becomes:

$$C(k^*) = 1 + \lambda [C_{QI}(k^*) + C_{FSI}(k^*)] \quad (8)$$

3.2 Momentum Resolution Corrections

Finite track momentum resolution causes the reconstructed momentum of a particle to smear around the true value. This, of course, also holds true for V0 particles. The effect is propagated up to the pairs of interest, which causes the reconstructed relative momentum (k_{Rec}^*) to differ from the true momentum (k_{True}^*). Smearing of the momentum typically will result in a suppression of the signal.

The effect of finite momentum resolution can be investigated using the MC data, for which both the true and reconstructed momenta are available.

Information gained from looking at k_{Rec}^* vs k_{True}^* can be used to apply corrections to account for the effects of finite momentum resolution on the correlation functions.

A second approach is to use information gained from response matrices. The response matrix describes quantitatively how each k_{Rec}^* bin receives contributions from multiple k_{True}^* bins, and can be used to account for the effects of finite momentum resolution. With this approach, the resolution correction is applied on-the-fly during the fitting process by propagating the theoretical (fit) correlation function through the response matrix, according to:

$$C_{fit}(k_{Rec}^*) = \frac{\sum_{k_{True}^*} M_{k_{Rec}^*, k_{True}^*} C_{fit}(k_{True}^*)}{\sum_{k_{True}^*} M_{k_{Rec}^*, k_{True}^*}} \quad (9)$$

where $M_{k_{Rec}^*, k_{True}^*}$ is the response matrix, $C_{fit}(k_{True}^*)$ is the fit binned in k_{True}^* , and the denominator normalizes the result.

Equation 9 describes that, for a given k_{Rec}^* bin, the observed value of $C(k_{Rec}^*)$ is a weighted average of all $C(k_{True}^*)$ values, where the weights are the normalized number of counts in the $[k_{Rec}^*, k_{True}^*]$ bin.

3.3 Residual Correlations

The purpose of this analysis is study the interaction and scale of the emitting source of the pairs. In order to obtain correct results, it is important for our particle collections to consist of primary particles. In practice, this is difficult to achieve for our Λ and $\bar{\Lambda}$ collections. Many of our Λ particles are not primary, but originate as decay products from other hyperons, including Σ^0 , Ξ^0 , Ξ^- and $\Sigma^{*(+, -, 0)}(1385)$.

Additionally, many of our K particles are not primary, but decay from $K^{*(+,-,0)}(892)$ parents. In these decays, the Λ carries away a momentum very similar to that of its parent. As a result, the correlation function between a secondary Λ and, for instance, a K^+ will be sensitive to, and dependent upon, the interaction between the parent of the Λ and the K^+ . In effect, the correlation between the parent of the Λ and the K^+ (ex. $\Sigma^0 K^+$) will be visible, although smeared out, in the ΛK^+ data. We call this a residual correlation resulting from feed-down. Residual correlations are important in an analysis when three criteria are met [15]: i) the parent correlation signal is large, ii) a large fraction of pairs in the sample originate from the particular parent system, and iii) the decay momenta are comparable to the expected correlation width in k^* .

As it is difficult for us to eliminate these residual correlations in our analyses, we must attempt to account for them in our fit. To achieve this, we model the correlation function of the parents, and run the correlation function through the appropriate transform matrix to determine the contribution to the daughter correlation function. The transform matrix describes the decay kinematics, and maps the k^* of the parent pair to that of the daughter. Finally, the primary correlation function, along with all contributions from residuals, are combined to form the complete correlation function. This process, for a ΛK correlation function with example contribution from a $\Sigma^0 K$ residual, is described in Eq. 10

$$\begin{aligned} C_{measured}(k_{\Lambda K}^*) &= 1 + \lambda_{\Lambda K}[C_{\Lambda K}(k_{\Lambda K}^*) - 1] + \lambda_{\Sigma^0 K}[C_{\Sigma^0 K}(k_{\Lambda K}^*) - 1] + \dots \\ &\quad + \lambda_{P_1 P_2}[C_{P_1 P_2}(k_{\Lambda K}^*) - 1] + \lambda_{other}[C_{other}(k_{\Lambda K}^*) - 1] \\ C_{P_1 P_2}(k_{\Lambda K}^*) &\equiv \frac{\sum_{k_{P_1 P_2}^*} C_{P_1 P_2}(k_{P_1 P_2}^*) T(k_{P_1 P_2}^*, k_{\Lambda K}^*)}{\sum_{k_{P_1 P_2}^*} T(k_{P_1 P_2}^*, k_{\Lambda K}^*)} \end{aligned} \quad (10)$$

$C_{\Sigma^0 K^+}(k_{\Sigma^0 K^+}^*)$ is the $\Sigma^0 K^+$ correlation function, and T is the transform matrix. This can be written more compactly as:

$$C_{measured}(k_{\Lambda K}^*) = 1 + \sum_i \lambda_i [C_i(k_{\Lambda K}^*) - 1] \quad (11)$$

The transform matrix generated with THERMINATOR [16], and is formed for a given parent pair, AB, by taking all ΛK pairs originating from AB, calculating the relative momentum of the parents (k_{AB}^*) and daughters ($k_{\Lambda K}^*$), and filling a two-dimensional histogram with the values. The transform matrix is essentially an unnormalized probability distribution mapping the k^* of the parent pair to that of the daughter pair when one or both parents decay.

The λ parameters roughly dictate the strength of the parent contribution to the daughter pair. Additionally, as found in [17], the reconstruction efficiency for primary Λ particles is nearly equal to that of Λ particles originating from Σ , Σ^* , Ξ^0 , Ξ^- , and Ω hyperons. Therefore, the λ parameter for parent system AB can be estimated using THERMINATOR as the total number of ΛK pairs originating from AB (N_{AB}) divided by the total number of ΛK pairs (N_{Total}):

$$\lambda_{AB} = \frac{N_{AB}}{N_{Total}} \quad (12)$$

The λ parameters used for this study can be found in Tab. A.1 in Appendix A.

Now, on to the question of how we model the parent correlation functions. In an ideal world, we would simply look up the parent interaction in some table, and input this into our model. Unfortunately, the

world in which we live is not perfect, such a table does not exists, and little is know about the interaction between the particles in the residual pairs of this study. Additionally, introducing a unique set of scattering parameters and radii for each residual system would introduce a large number of additional fit parameters, for which we do not have many constraints, and would cause our fitter to be too unconstrained and yield untrustworthy results. For this analysis, we assume all residual pairs have the same source size as the daughter pair. Furthermore, we assume Coulomb-neutral residual pairs share the same scattering parameters as the daughter pair.

For residual pairs affected by both the strong and Coulomb interactions, things are a bit more complicated. This is due to the fact that, for the case of both strong and Coulomb interaction, we no longer have a nice analytical form with which to fit. Generating a correlation function including both is also time consuming, as described further in Appendix B. Therefore, to treat this case, we have two different methods. First, we can use our experimental $\Xi^- K^\pm$ data to represent the charged parent pair system. Alternatively, we can assume the strong interaction is negligible in the charged residual, and generate the parent correlation function given radius and λ parameters (see Appendix B for more details). We find in our $\Xi^- K^\pm$ study that a Coulomb-only description of the system describes, reasonably well, the broad features of the correlation. The strong interaction is necessary for the fine details. However, as these correlations are run through a transform matrix, which largely flattens out and fine details, a Coulomb-only description should be sufficient. We find consistent results between using the ΞK data and the Coulomb-only interpolation method. When modeling $\Xi^- K^\pm$ residual correlations, we use the experimental $\Xi^- K^\pm$ data; in this case, there is no need to make any assumptions about scattering parameters or source sizes, as we already have the experimental data. When the number of residual pairs used is increased to 10, so that additional charged residual pairs such as $\Sigma^{*+} K^-$ enter the picture, the Coulomb-only interpolation method is used. Heh

3.4 Non-Flat Background

We observe a significant non-femtoscopic, non-flat, background in all of our correlations at large k^* . This background increases with decreasing centrality, is the same amongst all ΛK^\pm pairs, and is more pronounced in the ΛK_S^0 system. This difference in ΛK^\pm and ΛK_S^0 backgrounds is due mainly to the difference in kinematic cuts, not due to any interesting physics.

It is suggested that this background effect is due primarily to particle collimation associated with elliptic flow [18]. More specifically, these backgrounds result from mixing events with unlike event-plane angles (Ψ_{EP}). As explained in [18], when elliptic flow is present, all particles are more likely to be emitted in a specific direction (in-plane), as opposed to a perpendicular direction. Therefore, the difference in momenta for pairs of particles tends to be smaller, compared to the case of no flow. In the case of mixed-event pairs, the two events used do not share an event-plane, and therefore there is no collimation effect in the pairs from flow. As a result, pairs with larger momentum are more likely when mixed-events are used, causing the correlation function to be observed below unity. In general, a dip below unity, at a given k^* , means it is more probable to find a pair at that k^* when the daughters are taken from mixed-events, as compared to when they are taken from the same event.

This same reasoning suggests that the background should lead to an enhancement at low- k^* . The enhancement at high- k^* ($k^* \gtrsim 1.5$ GeV/c) does not result from the collective flow of the system. We are not certain what causes this enhancement, but typical suspects are jet-like correlations and resonance decays.

THERMINATOR 2 simulation has been shown to reproduce the background features in a πK analysis [18]. As the background effect can be attributed mainly to elliptic flow, which is a global feature of the system, we suspected THERMINATOR 2 could also, at least qualitatively, describe our backgrounds. After ensuring each simulated event received a random event-plane angle (Ψ_{EP}), we found THERMINATOR 2 did a good job of describing our data qualitatively, and, in many cases, quantitatively.

3.5 LednickyFitter

A simple χ^2 test is inappropriate for fitting correlation functions, as the ratio two Poisson distributions does not result in a Poisson distribution. Instead, a log-likelihood fit function of the following form is used [1]:

$$\chi_{PML}^2 = -2 \left[A \ln \left(\frac{C(A+B)}{A(C+1)} \right) + B \ln \left(\frac{A+B}{B(C+1)} \right) \right] \quad (13)$$

where A is the experimental signal distribution (numerator), B is the experimental background distribution (denominator), and C is the theoretical fit correlation function.

The fitter uses Equations 5 – 7 to build the theoretical fit, and Equation 13 as the statistic quantifying the quality of the fit. The parameters of the fit are: λ , R , f_0 ($\mathbb{R}f_0$ and $\mathbb{I}f_0$ separately), d_0 , and normalization N . The fitter currently includes methods to correct for momentum resolution and a non-flat background. These corrections are applied to the fit function, the data is never touched. The fitter is able to share parameters between different analyses and fit all simultaneously.

In a typical fit, a given pair is fit with its conjugate (ex. ΛK^+ with $\bar{\Lambda} K^-$) across all centralities (0-10%, 10-30%, 30-50%), for a total of 6 simultaneous analyses. Each analysis has a unique λ and normalization parameter. The radii are shared between analyses of like centrality, as these should have similar source sizes. The scattering parameters ($\mathbb{R}f_0$, $\mathbb{I}f_0$, d_0) are shared amongst all.

In the case of fitting with residuals, the λ_{Fit} parameter serves as an overall normalization shared by all contributors, such that Eqn 11 becomes:

$$\begin{aligned} C_{measured}(k_{\Lambda K}^*) &= 1 + \sum_i \lambda'_i [C_i(k_{\Lambda K}^*) - 1] \\ \lambda'_i &= \lambda_{Fit} \lambda_i \\ \sum_i \lambda'_i &= \lambda_{Fit} \sum_i \lambda_i = \lambda_{Fit} \end{aligned} \quad (14)$$

where λ_i is obtained from THERMINATOR, as explained in Section 3.3, and whose values are presented in Tables ?? through ?. For Coulomb-neutral pairs, such as ΛK , $\Sigma^0 K$, and $\Xi^0 K$, $C_i(k_{\Lambda K}^*)$ is calculated from Eqn. 5, with the help of Eqn. 7. For those residual pairs which include a Coulomb interaction, $C_i(k_{\Lambda K}^*)$ is either calculated assuming no strong interaction, or by using the $\Xi^{ch} K^{ch}$ data directly. Unless otherwise stated, the $\Xi^{ch} K^{ch}$ residual contribution is modeled using the experimental $\Xi^{ch} K^{ch}$ data, and all other charged contributors (ex. $\Sigma^{*ch} K^{ch}$) are modeled using the Coulomb-only technique with no strong interaction contribution.

To summarize, the complete fit function is constructed as follows:

1. The uncorrected, primary, correlation function, $C_{\Lambda K}(k_{\text{True}}^*)$, is constructed using Eq. 15 (with the help of Eqns. 5 and 7)
2. If residuals are included:
 - the parent correlation functions are obtained using:
 - Eq. 15 (with the help of Eqns. 5 and 7) for the case of Coulomb-neutral pairs
 - $\Xi^- K^\pm$ experimental data for $\Xi^- K^\pm$ contributions
 - a Coulomb-only curve, with the help of Secs. ?? and ??, for pairs including the Coulomb interaction

- the contribution to the ΛK correlation function is found by running the parent correlation function through the appropriate transform, via Eq.10
3. The primary and residual correlations are combined, via Eq.11, to form $C'_{Fit}(k^*_{True})$
 - in the case of no residual contributions included in the fit, $\lambda_i = \lambda_{\Lambda K}$ in Eq. 15 is set equal to 1. Then, the extracted λ_{Fit} parameter should be roughly equal to the pair purity
 - when residuals are included, the λ_i values are presented in Table A.1
 4. The correlation function is corrected to account for momentum resolution effects using Eq. 9

$$- C'_{Fit}(k^*_{Rec}) = \frac{\sum_{k^*_{True}} M_{k^*_{Rec}, k^*_{True}} C'_{Fit}(k^*_{True})}{\sum_{k^*_{True}} M_{k^*_{Rec}, k^*_{True}}}$$

5. Finally, the non-flat background correction is applied, and the final fit function is obtained

$$- C_{Fit}(k^*_{Rec}) = C'_{Fit}(k^*_{Rec}) * F_{Bgd}(k^*_{Rec})$$

3.6 Systematic uncertainties

In order to understand my systematic uncertainties, the analysis code was run many times using slightly different values for a number of important cuts, and the results were compared.

In order to quantify the systematic errors on the data, all correlation functions built using all varied cut values were bin-by-bin averaged, and the resulting variance of each bin was taken as the systematic error. The cuts which were utilized in this study are presented in Sections ?? (ΛK_S^0) and ?? (ΛK^\pm).

Similarly, the fit parameters extracted from all of these correlation functions were averaged, and the resulting variances were taken as the systematic errors for the fit parameters. As with the systematic errors on the data, this was performed for all varied cut values. Additionally, a systematic analysis was done on our fit method. These two sources of uncertainty were combined in quadrature to obtain the final systematic uncertainties on the extracted fit parameters.

The cuts included in the systematic study, as well as the values used in the variations, are shown in Tab. 4 (ΛK_S^0) and Tab. 5 (ΛK^\pm). Note, the central value corresponds to that used in the analysis.

We fit our non-flat background with a linear function. To study the contribution of this choice to our systematic errors, we also fit with a quadratic and Gaussian form. The resulting uncertainties are combined with the uncertainties arising from our particle cuts.

Our choice of k^* fit range was varied by $\pm 25\%$. The resulting uncertainties in the extracted parameter sets were combined with our uncertainties arising from our particle and pair cuts.

4 Results

Hooray, finally some results!

Figure 4 shows fits, with 3 residual correlations included, for all ΛK analyses across all studied centralities (0-10%, 10-30%, and 30-50%). For the ΛK_S^0 results, all analyses are fit simultaneously across all centralities. A single λ parameter is shared amongst all. Each analysis has a unique normalization parameter. The radii are shared between analyses of like centrality. The scattering parameters ($\mathbb{R}f_0$, $\mathbb{I}f_0$, d_0) are shared amongst all. For the ΛK^\pm results, all analyses are fit simultaneously across all centralities. Scattering parameters ($\mathbb{R}f_0$, $\mathbb{I}f_0$, d_0) are shared between pair-conjugate systems (i.e. a parameter set describing the ΛK^+ & $\bar{\Lambda} K^-$ system, and a separate set describing the ΛK^- & $\bar{\Lambda} K^+$ system). For

ΛK_S^0 systematics

ΛK_S^0 systematics	
DCA $\Lambda(\bar{\Lambda})$	4, 5, 6 mm
DCA K_S^0	2, 3, 4 mm
DCA $\Lambda(\bar{\Lambda})$ Daughters	3, 4, 5 mm
DCA K_S^0 Daughters	2, 3, 4 mm
$\Lambda(\bar{\Lambda})$ Cosine of Pointing Angle	0.9992, 0.9993, 0.9994
K_S^0 Cosine of Pointing Angle	0.9992, 0.9993, 0.9994
DCA to Primary Vertex of $p(\bar{p})$ Daughter of $\Lambda(\bar{\Lambda})$	0.5, 1, 2 mm
DCA to Primary Vertex of $\pi^-(\pi^+)$ Daughter of $\Lambda(\bar{\Lambda})$	2, 3, 4 mm
DCA to Primary Vertex of π^+ Daughter of K_S^0	2, 3, 4 mm
DCA to Primary Vertex of π^- Daughter of K_S^0	2, 3, 4 mm
Average Separation of Like-Charge Daughters	5, 6, 7 cm

Table 4: ΛK_S^0 systematics ΛK^\pm systematics

ΛK^\pm systematics	
DCA $\Lambda(\bar{\Lambda})$	4, 5, 6 mm
DCA $\Lambda(\bar{\Lambda})$ Daughters	3, 4, 5 mm
$\Lambda(\bar{\Lambda})$ Cosine of Pointing Angle	0.9992, 0.9993, 0.9994
DCA to Primary Vertex of $p(\bar{p})$ Daughter of $\Lambda(\bar{\Lambda})$	0.5, 1, 2 mm
DCA to Primary Vertex of $\pi^-(\pi^+)$ Daughter of $\Lambda(\bar{\Lambda})$	2, 3, 4 mm
Average Separation of $\Lambda(\bar{\Lambda})$ Daughter with Same Charge as K^\pm	7, 8, 9 cm
Max. DCA to Primary Vertex in Transverse Plane of K^\pm	1.92, 2.4, 2.88
Max. DCA to Primary Vertex in Longitudinal Direction of K^\pm	2.4, 3.0, 3.6

Table 5: ΛK^\pm systematics

each centrality, a radius and λ parameters are shared between all pairs (ΛK^+ , $\bar{\Lambda} K^-$, ΛK^- , $\bar{\Lambda} K^+$). Each analysis has a unique normalization parameter.

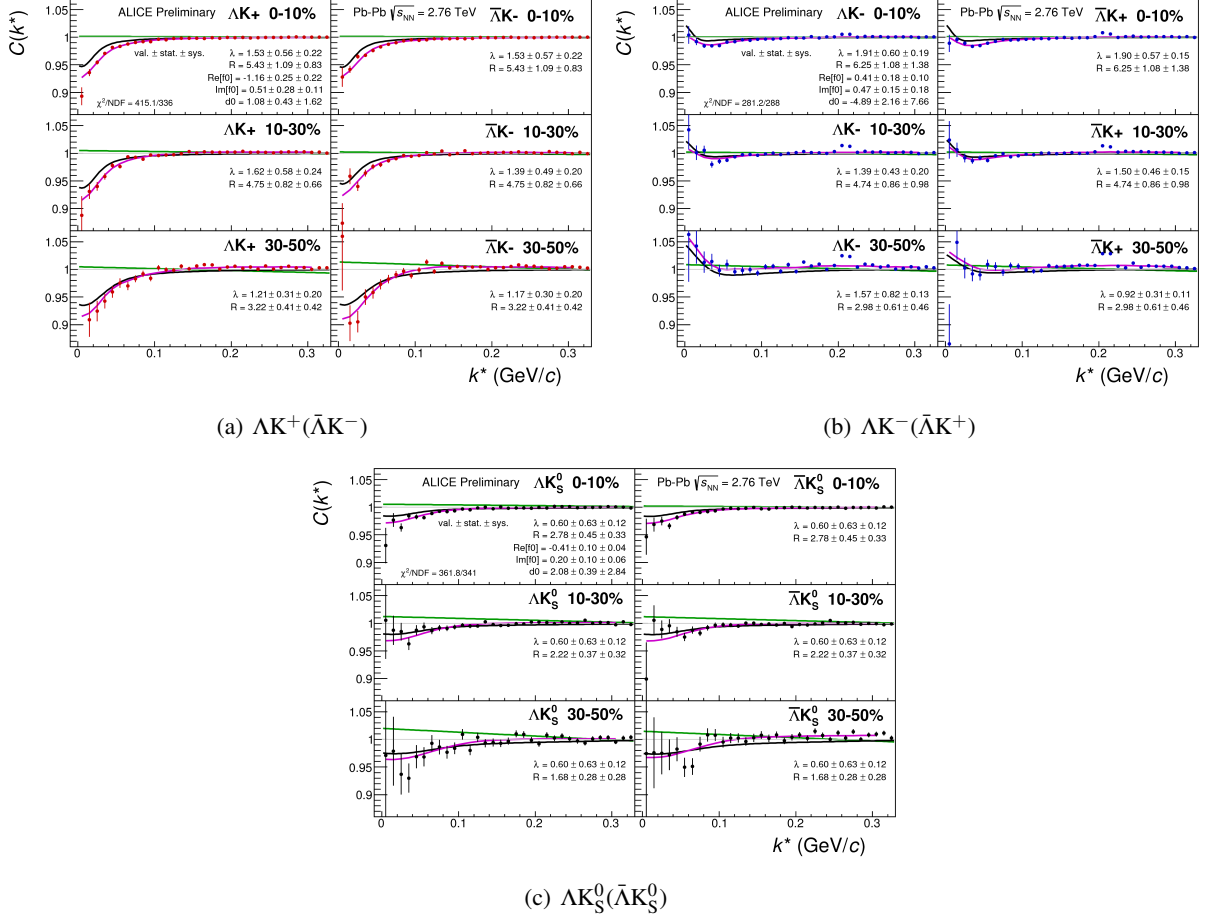


Fig. 4: Fits, with 3 residual correlations included, for all ΛK analyses across all studied centralities (0-10%, 10-30%, and 30-50%). The lines represent the statistical errors, while the boxes represent the systematic errors. The backgrounds are modeled by (6th-)degree polynomials fit to THERMINATOR simulation. The black solid line represents the primary (ΛK) correlation's contribution to the fit. The green line shows the fit to the non-flat background. The purple points show the fit after all residuals' contributions have been included, and momentum resolution and non-flat background corrections have been applied. The extracted fit values with uncertainties are printed.

5 Summary

We did physics, and we found physics.

Acknowledgements

References

- [1] M. A. Lisa, S. Pratt, R. Soltz, and U. Wiedemann, “Femtoscopy in relativistic heavy ion collisions,” *Ann. Rev. Nucl. Part. Sci.* **55** (2005) 357–402, arXiv:nucl-ex/0505014 [nucl-ex].
- [2] R. Lednický and V. L. Lyuboshitz *Sov. J. Nucl. Phys.* **35** (1982) 770.

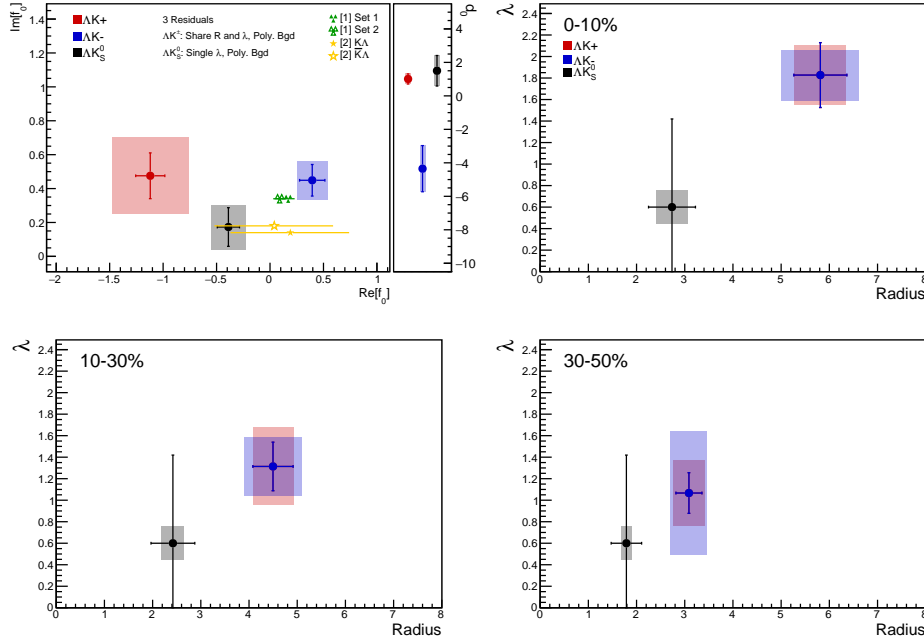


Fig. 5: Extracted scattering parameters for the case of 3 residual contributors for all of our ΛK systems. [Top Left]: $\text{Im}f_0$ vs. $\text{Re}f_0$, together with d_0 to the right. [Top Right (Bottom Left, Bottom Right)]: λ vs. Radius for the 0-10% (10-30%, 30-50%) bin. The green [19] and yellow [20] points show theoretical predictions made using chiral perturbation theory.

- [3] ALICE Collaboration, K. Aamodt *et al.*, “The alice experiment at the cern lhc,” *JINST* **3** (2008) S08002. <http://stacks.iop.org/1748-0221/3/i=08/a=S08002>.
- [4] ALICE Collaboration, B. Abelev *et al.*, “Centrality determination of Pb-Pb collisions at $\sqrt{s_{NN}} = 2.76$ TeV with ALICE,” *Phys. Rev.* **C88** no. 4, (2013) 044909, arXiv:1301.4361 [nucl-ex].
- [5] J. Alme *et al.*, “The ALICE TPC, a large 3-dimensional tracking device with fast readout for ultra-high multiplicity events,” *Nucl. Instrum. Meth. A* **622** (2010) 316–367, arXiv:1001.1950 [physics.ins-det].
- [6] ALICE Collaboration, G. Dellacasa *et al.*, *ALICE time projection chamber: Technical Design Report*. Technical Design Report ALICE. CERN, Geneva, 2000. <http://cds.cern.ch/record/451098>.
- [7] ALICE Collaboration, B. B. Abelev *et al.*, “Performance of the ALICE Experiment at the CERN LHC,” *Int. J. Mod. Phys. A* **29** (2014) 1430044, arXiv:1402.4476 [nucl-ex].
- [8] A. Akindinov *et al.*, “Performance of the ALICE Time-Of-Flight detector at the LHC,” *Eur. Phys. J. Plus* **128** (2013) 44.
- [9] ALICE Collaboration Collaboration, P. Cortese, *ALICE Time-Of Flight system (TOF): addendum to the Technical Design Report*. Technical Design Report ALICE. CERN, Geneva, 2002. <http://cds.cern.ch/record/545834>.
- [10] Particle Data Group Collaboration, C. Patrignani *et al.*, “Review of Particle Physics,” *Chin. Phys. C* **40** no. 10, (2016) 100001.
- [11] X.-N. Wang and M. Gyulassy, “hijing: A monte carlo model for multiple jet production in pp, pA, and AA collisions,” *Phys. Rev. D* **44** (Dec, 1991) 3501–3516. <https://link.aps.org/doi/10.1103/PhysRevD.44.3501>.

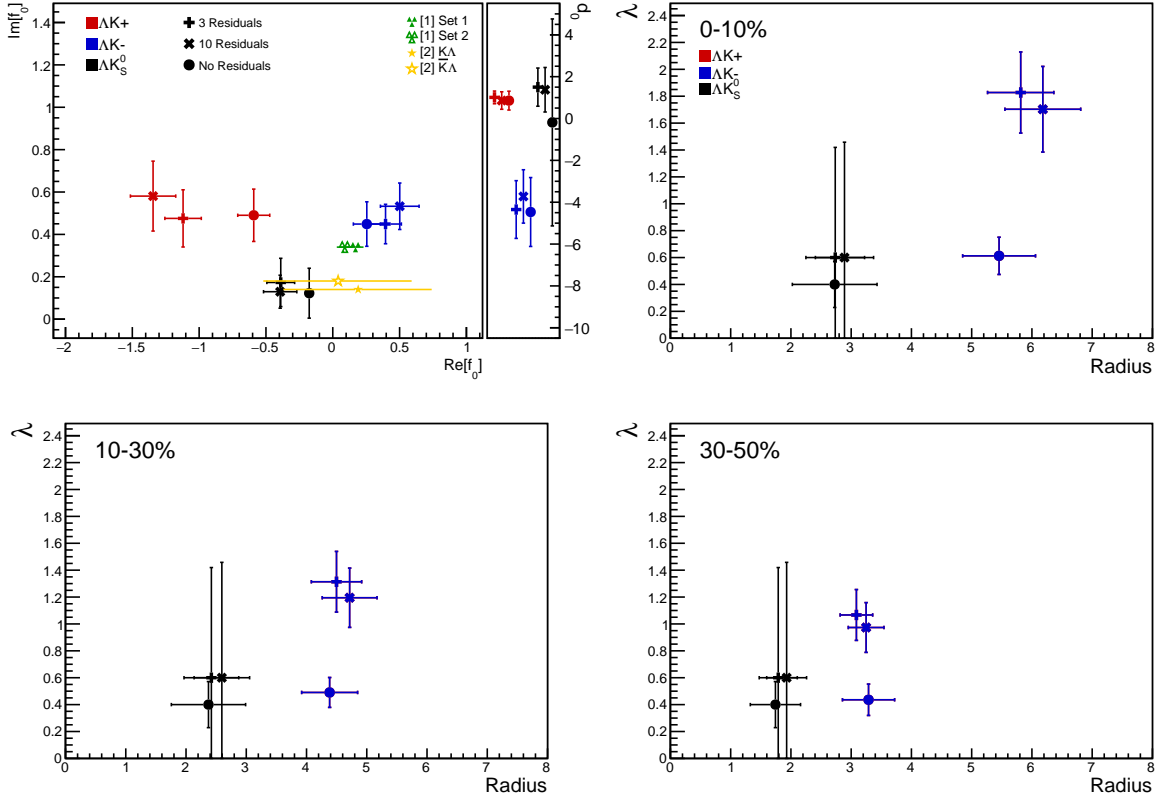


Fig. 6: Compare Fit Parameters: Number of residuals: Results shown for the case of 3 (+), 10 (X), and no (circles) residual contributors.

- [12] R. Brun, F. Bruyant, F. Carminati, S. Giani, M. Maire, A. McPherson, G. Patrick, and L. Urban, “GEANT Detector Description and Simulation Tool,”.
- [13] S. E. Koonin, “Proton Pictures of High-Energy Nuclear Collisions,” *Phys. Lett.* **B70** (1977) 43–47.
- [14] S. Pratt, T. Csorgo, and J. Zimanyi, “Detailed predictions for two pion correlations in ultrarelativistic heavy ion collisions,” *Phys. Rev.* **C42** (1990) 2646–2652.
- [15] A. Kisiel, H. Zbroszczyk, and M. Szymaski, “Extracting baryon-antibaryon strong interaction potentials from $p\bar{\Lambda}$ femtoscopic correlation functions,” *Phys. Rev.* **C89** no. 5, (2014) 054916, arXiv:1403.0433 [nucl-th].
- [16] M. Chojnacki, A. Kisiel, W. Florkowski, and W. Broniowski, “THERMINATOR 2: THERMal heavy IoN generATOR 2,” *Comput. Phys. Commun.* **183** (2012) 746–773, arXiv:1102.0273 [nucl-th].
- [17] J. Salzwedel and T. Humanic, “Lambda femtoscopy in $\sqrt{s_{NN}} = 2.76$ TeV Pb-Pb collisions at ALICE,” Jan, 2017. <http://cds.cern.ch/record/2241303>. Presented 15 Dec 2016.
- [18] A. Kisiel, “Non-identical particle correlation analysis in the presence of non-femtoscopic correlations,” *Acta Physica Polonica B* **48** (04, 2017) 717.
- [19] Y.-R. Liu and S.-L. Zhu, “Meson-baryon scattering lengths in HB chi PT,” *Phys. Rev.* **D75** (2007) 034003, arXiv:hep-ph/0607100 [hep-ph].

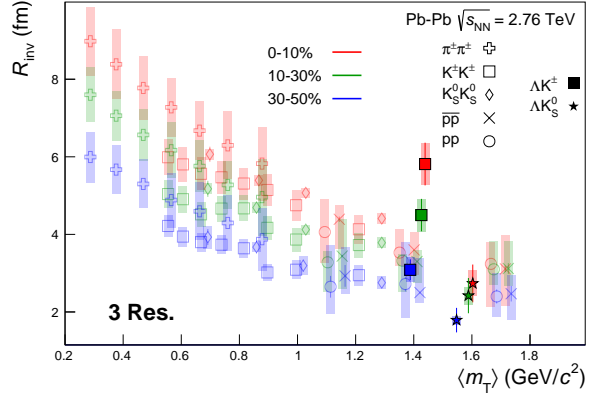


Fig. 7: 3 residual correlations in ΛK fits. Extracted fit R_{inv} parameters as a function of pair transverse mass (m_T) for various pair systems over several centralities. The ALICE published data [21] is shown with transparent, open symbols. The new ΛK results are shown with opaque, filled symbols. In the left, the ΛK^+ (with its conjugate pair) results are shown separately from the ΛK^- (with its conjugate pair) results. In the right, all ΛK^\pm results are averaged.

- [20] M. Mai, P. C. Bruns, B. Kubis, and U.-G. Meissner, “Aspects of meson-baryon scattering in three and two-flavor chiral perturbation theory,” *Phys. Rev.* **D80** (2009) 094006, arXiv:0905.2810 [hep-ph].
- [21] **ALICE Collaboration**, J. Adam *et al.*, “One-dimensional pion, kaon, and proton femtoscopy in Pb-Pb collisions at $\sqrt{s_{\text{NN}}} = 2.76 \text{ TeV}$,” *Phys. Rev.* **C92** no. 5, (2015) 054908, arXiv:1506.07884 [nucl-ex].
- [22] R. Lednicky, “Finite-size effects on two-particle production in continuous and discrete spectrum,” *Phys. Part. Nucl.* **40** (2009) 307–352, arXiv:nucl-th/0501065 [nucl-th].

A λ Parameters

AK ⁺ residuals		$\bar{A}K^-$ residuals		AK ⁻ residuals		$\bar{A}K^+$ residuals		AK _S ⁰ residuals		$\bar{A}K_S^0$ residuals	
Pair System	λ value	Pair System	λ value	Pair System	λ value	Pair System	λ value	Pair System	λ value	Pair System	λ value
3 Residuals											
AK ⁺	0.154	$\bar{A}K^-$	0.158	AK ⁻	0.154	$\bar{A}K^+$	0.158	AK _S ⁰	0.165	$\bar{A}K_S^0$	0.169
$\Sigma^0 K^+$	0.099	$\bar{\Sigma}^0 K^-$	0.102	$\Sigma^0 K^-$	0.099	$\bar{\Sigma}^0 K^+$	0.103	$\Sigma^0 K_S^0$	0.107	$\bar{\Sigma}^0 K_S^0$	0.111
$\Xi^0 K^+$	0.072	$\bar{\Xi}^0 K^-$	0.067	$\Xi^0 K^-$	0.071	$\bar{\Xi}^0 K^+$	0.068	$\Xi^0 K_S^0$	0.077	$\bar{\Xi}^0 K_S^0$	0.073
$\Xi^- K^+$	0.069	$\bar{\Xi}^+ K^-$	0.065	$\Xi^- K^-$	0.068	$\bar{\Xi}^+ K^+$	0.066	$\Xi^- K_S^0$	0.075	$\bar{\Xi}^+ K_S^0$	0.071
Other	0.558	Other	0.560	Other	0.561	Other	0.557	Other	0.528	Other	0.528
Fakes	0.048	Fakes	0.048	Fakes	0.048	Fakes	0.048	Fakes	0.048	Fakes	0.048
10 Residuals											
AK ⁺	0.154	$\bar{A}K^-$	0.158	AK ⁻	0.154	$\bar{A}K^+$	0.158	AK _S ⁰	0.165	$\bar{A}K_S^0$	0.169
$\Sigma^0 K^+$	0.099	$\bar{\Sigma}^0 K^-$	0.102	$\Sigma^0 K^-$	0.099	$\bar{\Sigma}^0 K^+$	0.103	$\Sigma^0 K_S^0$	0.107	$\bar{\Sigma}^0 K_S^0$	0.111
$\Xi^0 K^+$	0.072	$\bar{\Xi}^0 K^-$	0.067	$\Xi^0 K^-$	0.071	$\bar{\Xi}^0 K^+$	0.068	$\Xi^0 K_S^0$	0.077	$\bar{\Xi}^0 K_S^0$	0.073
$\Xi^- K^+$	0.069	$\bar{\Xi}^+ K^-$	0.065	$\Xi^- K^-$	0.068	$\bar{\Xi}^+ K^+$	0.066	$\Xi^- K_S^0$	0.075	$\bar{\Xi}^+ K_S^0$	0.071
$\Sigma^{*+} K^+$	0.046	$\bar{\Sigma}^{*-} K^-$	0.046	$\Sigma^{*+} K^-$	0.046	$\bar{\Sigma}^{*-} K^+$	0.046	$\Sigma^{*+} K_S^0$	0.050	$\bar{\Sigma}^{*-} K_S^0$	0.050
$\Sigma^{*-} K^+$	0.042	$\bar{\Sigma}^{*+} K^-$	0.045	$\Sigma^{*-} K^-$	0.041	$\bar{\Sigma}^{*+} K^+$	0.045	$\Sigma^{*-} K_S^0$	0.045	$\bar{\Sigma}^{*+} K_S^0$	0.049
$\Sigma^{*0} K^+$	0.042	$\bar{\Sigma}^{*0} K^-$	0.040	$\Sigma^{*0} K^-$	0.041	$\bar{\Sigma}^{*0} K^+$	0.041	$\Sigma^{*0} K_S^0$	0.045	$\bar{\Sigma}^{*0} K_S^0$	0.044
ΛK^{*0}	0.039	$\bar{\Lambda} \bar{K}^{*0}$	0.041	$\Lambda \bar{K}^{*0}$	0.039	$\bar{\Lambda} K^{*0}$	0.041	ΛK^{*0}	0.019	$\bar{\Lambda} K^{*0}$	0.020
$\Sigma^0 K^{*0}$	0.035	$\bar{\Sigma}^0 \bar{K}^{*0}$	0.036	$\Sigma^0 \bar{K}^{*0}$	0.035	$\bar{\Sigma}^0 K^{*0}$	0.036	$\Sigma^0 K^{*0}$	0.017	$\bar{\Sigma}^0 K^{*0}$	0.017
$\Xi^0 K^{*0}$	0.025	$\bar{\Xi}^0 \bar{K}^{*0}$	0.024	$\Xi^0 \bar{K}^{*0}$	0.025	$\bar{\Xi}^0 K^{*0}$	0.024	$\Xi^0 K^{*0}$	0.012	$\bar{\Xi}^0 K^{*0}$	0.011
$\Xi^- K^{*0}$	0.024	$\bar{\Xi}^+ \bar{K}^{*0}$	0.023	$\Xi^- \bar{K}^{*0}$	0.024	$\bar{\Xi}^+ K^{*0}$	0.023	$\Xi^- K^{*0}$	0.012	$\bar{\Xi}^+ K^{*0}$	0.011
Other	0.305	Other	0.305	Other	0.308	Other	0.301	Other	0.329	Other	0.326
Fakes	0.048	Fakes	0.048	Fakes	0.048	Fakes	0.048	Fakes	0.048	Fakes	0.048

Table A.1: λ values for the individual components of the AK correlation functions for the case of 3 and 10 residual contributions.

B Strong and Coulomb Fitter

When modeling systems which include both strong and Coulomb effects, Eq. 5 is no longer valid, and, in fact, there is no analytical form with which to fit. Therefore, we must begin with the wave function describing the pair interaction, and simulate many particle pairs to obtain a theoretical fit correlation function. Unfortunately, the nature of this process means that the run time increases dramatically.

The two-particle correlation function may be written as:

$$C(\mathbf{k}^*) = \sum_S \rho_S \int S(\mathbf{r}^*) |\Psi_{\mathbf{k}^*}^S(\mathbf{r}^*)|^2 d^3 \mathbf{r}^* \quad (\text{B.1})$$

where ρ_S is the normalized emission probability of particles in a state with spin S , $S(\mathbf{r}^*)$ is the pair emission source distribution (assumed to be Gaussian), and $\Psi_{\mathbf{k}^*}^S(\mathbf{r}^*)$ is the two-particle wave-function including both strong and Coulomb interactions [22]:

$$\Psi_{\mathbf{k}^*}(\mathbf{r}^*) = e^{i\delta_c} \sqrt{A_c(\eta)} [e^{i\mathbf{k}^* \cdot \mathbf{r}^*} F(-i\eta, 1, i\xi) + f_c(k^*) \frac{\tilde{G}(\rho, \eta)}{r^*}] \quad (\text{B.2})$$

where $\rho = k^* r^*$, $\eta = (k^* a_c)^{-1}$, $\xi = \mathbf{k}^* \cdot \mathbf{r}^* + k^* r^* \equiv \rho(1 + \cos \theta^*)$, and $a_c = (\mu z_1 z_2 e^2)^{-1}$ is the two-particle Bohr radius (including the sign of the interaction). δ_c is the Coulomb s-wave phase shift, $A_c(\eta)$ is the Coulomb penetration factor, $\tilde{G} = \sqrt{A_c}(G_0 + iF_0)$ is a combination of the regular (F_0) and singular (G_0) s-wave Coulomb functions. $f_c(k^*)$ is the s-wave scattering amplitude:

$$f_c(k^*) = [\frac{1}{f_0} + \frac{1}{2} d_0 k^{*2} - \frac{2}{a_c} h(\eta) - ik^* A_c(\eta)]^{-1} \quad (\text{B.3})$$

where, the “h-function”, $h(\eta)$, is expressed through the digamma function, $\psi(z) = \Gamma'(z)/\Gamma(z)$ as:

$$h(\eta) = 0.5[\psi(i\eta) + \psi(-i\eta) - \ln(\eta^2)] \quad (\text{B.4})$$

In this case, the λ parameter may be included as:

$$C(\mathbf{k}^*) = (1 - \lambda) + \lambda \sum_S \rho_S \int S(\mathbf{r}^*) |\Psi_{\mathbf{k}^*}^S(\mathbf{r}^*)|^2 d^3 \mathbf{r}^* \quad (\text{B.5})$$

To generate a fit correlation function, we must simulate a large number of pairs, calculate the wave-function, and average Ψ^2 over all pairs in a given \mathbf{k}^* bin. Essentially, we calculate Equation B.1 by hand:

$$\begin{aligned} C(\mathbf{k}^*) &= \sum_S \rho_S \int S(\mathbf{r}^*) |\Psi_{\mathbf{k}^*}^S(\mathbf{r}^*)|^2 d^3 \mathbf{r}^* \\ &\longrightarrow C(|\mathbf{k}^*|) \equiv C(k^*) = \sum_S \rho_S \langle |\Psi^S(\mathbf{k}_i^*, \mathbf{r}_i^*)|^2 \rangle_i \\ &\longrightarrow C(k^*) = \lambda \sum_S \rho_S \langle |\Psi^S(\mathbf{k}_i^*, \mathbf{r}_i^*)|^2 \rangle_i + (1 - \lambda) \end{aligned} \quad (\text{B.6})$$

where $\langle \rangle_i$ represents an average over all pairs in a given \mathbf{k}^* bin.

In summary, for a given \mathbf{k}^* bin, we must draw $N_{pairs} \sim 10^4$ pairs, and for each pair:

1. Draw a random \mathbf{r}^* vector according to our Gaussian source distribution $S(\mathbf{r}^*)$
2. Draw a random \mathbf{k}^* vector satisfying the $|\mathbf{k}^*|$ restriction of the bin
 - We draw from real k^* vectors obtained from the data
 - However, we find that drawing from a distribution flat in k^* gives similar results
3. Construct the wave-function Ψ

After all pairs for a given k^* bin are simulated and wave-functions obtained, the results are averaged to give the fit result.

C The ALICE Collaboration